Crystal Phase Induced Bandgap Modifications in AlAs Nanowires Probed by Resonant Raman Spectroscopy

Stefan Funk,[†,‡,*] Ang Li,[§] Daniele Ercolani,[§] Mauro Gemmi,[⊥] Lucia Sorba,[§] and Ilaria Zardo[†,‡,¶]

[†]Walter Schottky Institut and Physik Department, Technische Universität München, D-85748 Garching, Germany, [‡]Institute for Advanced Study, Technische Universität München, D-85748 Garching, Germany, [§]NEST, Istituto Nanoscienze-CNR and Scuola Normale Superiore, I-56127 Pisa, Italy, and [⊥]Center for Nanotechnology Innovation @ NEST, Istituto Italiano di Tecnologia, I-56127 Pisa, Italy. *Present address: Applied Physics, Photonics & Semiconductor Nanophysics, Eindhoven University of Technology, MB 5600 Eindhoven, The Netherlands.

ABSTRACT We report on a major modification of the fundamental electronic band structure of AlAs when grown as a nanoscaled wurtzite crystal. Resonant Raman spectra of individual AlAs–GaAs core–shell nanowires display a resonance between 1.83 and 2.18 eV for the AlAs E_1(TO) phonon mode. Our findings substantiate the lowest conduction band of wurtzite AlAs to comprise Γ_8 symmetry and a low effective mass in agreement with calculations reported recently. The electronic resonance falls below the X, L, and Γ valleys known for AlAs in the zincblende phase. This result points toward a direct nature of wurtzite AlAs and is expected to apply more generally to semiconductors that in the bulk phase exhibit L valleys at lower energies than the conduction band at the Γ point.

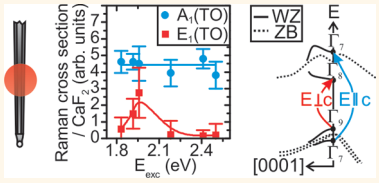

KEYWORDS: AlAs nanowires · wurtzite · electronic band structure · resonant Raman spectroscopy

A structural novelty observed in semiconductor nanowires (NWs) based on III–V semiconductor compounds is their favored crystallization in the hexagonal wurtzite (WZ) phase.[1−3] This finding contrasts with related bulk counterparts that occur in the zincblende (ZB) phase and is inherently accompanied by diversified phonon and electron dispersions that recently introduced a new class of semiconductor heterostructures where variations in the stacking order give rise to axially defined crystal phase quantum dots.[4−6] The novel heterostructures displayed atomically sharp interfaces and a type II band alignment. Hence, they hold great promise in quantum computing and photovoltaics.[5] Bandgap modifications experimentally found in common III–V direct semiconductors such as GaAs and InAs range typically below 50 meV.[7−9] Here, the related small band offsets may limit the technological importance of related crystal phase junctions especially at elevated temperatures due to reduced charge carrier confinement and separation. On the other hand, recent theoretical works suggest that certain indirect semiconductors such as AlAs, AlP, and GaP may display a much more drastic change of their electronic bands when transferred from the cubic to the hexagonal crystal phase.[10,11] In the case of AlAs, A. De *et al*. predict a reduction of the fundamental bandgap at the Γ point of the first Brillouin zone from approximately 3 to 2 eV due to the introduction of a backfolded conduction band of Γ_8 symmetry and hereby claim WZ AlAs to exhibit a direct bandgap.[10]

Certainly, the implications of such major modifications of electronic bands would be vast in nanotechnology: first, knowledge on the actual value and nature of the fundamental bandgap in WZ AlAs plays a crucial role for the design of future GaAs–$Al_xGa_{1-x}As$–AlAs-based nanoscaled heterojunctions that are currently investigated for their potential in electronics and photonics.[12−17] Second, a direct nature of the fundamental bandgap would suggest WZ AlAs itself as a novel optically active material in the visible light region. In this regard, a special emphasis can be placed to the large expected bandgap offset between AlAs in the WZ and ZB phase that would substantially exceed values reported in other material systems. However,

* Address correspondence to stefan.funk@wsi.tum.de.

Received for review November 2, 2012 and accepted January 2, 2013.

Published online January 02, 2013
10.1021/nn305112a

the assumption of a direct bandgap below 2 eV in WZ AlAs is currently a matter of debate since earlier calculations based on the local-density approximation did not reveal a direct bandgap.[18] Additionally, literature currently lacks any experimental investigation on the optical properties of WZ AlAs. This may be reasoned by the fact that the growth of WZ AlAs NWs has been accomplished just recently.[19]

Resonant Raman (RR) spectroscopy has been established as a versatile probe for both the structural and electronic properties of semiconductors.[20−22] In particular, RR spectroscopy has been successfully applied to resolve the lattice dynamics and electronic bandstructure of semiconductor NWs.[7,8,23] The method relies on the dependence of the Raman cross section on the energy difference between incoming photons impinging on a crystal and absorption centers caused by interband critical points such as the fundamental bandgap E_0. Hence, by examining the excitation-dependent Raman cross section of distinct vibrational modes, one is able to obtain valuable information on the energetic values, dispersions, and symmetries of the bands involved in an optical transition. A particular advantage is the local nature of RR spectroscopy: Excited electron−hole pairs involved in the Raman process have not been diffusing toward regions displaying a lower joint density of states prior to their recombination. This is of particular advantage when electronic properties of materials incorporated in nanoscaled heterostructures are examined where the fundamental bandgap of the material under investigation is bigger than adjacent layers.

In this manuscript, we study the RR spectrum of individual AlAs−GaAs core−shell nanowires (C−S NWs) in the WZ crystal phase. We resolve the TO splitting that results in WZ AlAs related TO phonon modes with A_1 and E_1-symmetry. In particular, we investigate a resonant effect of the E_1(TO) mode between 1.83 and 2.18 eV in WZ AlAs. The experimental results show the presence of a minor dispersive conduction band of Γ_8 symmetry arising due to the hexagonal crystal phase.

RESULTS AND DISCUSSION

Structural Properties and Vibrational Modes. A typical image of an individual AlAs−GaAs C−S NW obtained by bright field transmission electron microscopy (TEM) is displayed in Figure 1a. On the right-hand side, we observe the top of the C−S NW incorporating the gold catalyst and a short axial ZB GaAs segment underneath that is introduced during shell overgrowth.[19] To detect the crystal phase of the C−S NW we collected electron diffraction patterns at the center and on areas of 150 nm in diameter near the two extremes in the [$2\bar{1}\bar{1}0$] orientation where WZ and ZB diffraction patterns do not superimpose. The pattern taken at the center displays sharp spots in accordance with a WZ

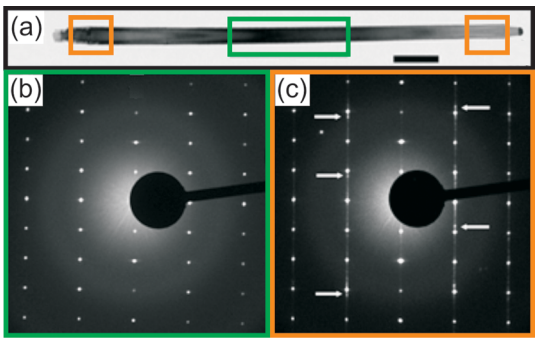

Figure 1. (a) Bright field TEM image of an AlAs−GaAs C−S NW. The black scale bar corresponds to 150 nm. (b) Selected area electron diffraction pattern taken in the central area of the NW oriented in the [$2\bar{1}\bar{1}0$] WZ zone axis. (c) Selected area diffraction pattern taken from an area of 150 nm in diameter close to the top of the NW oriented in [$2\bar{1}\bar{1}0$]. The white arrows indicate the maxima along the streaking corresponding to ZB spots. A similar pattern can be obtained at the bottom of the wire.

structure (see Figure 1b), while those taken at the top and the bottom show streaking along the WZ spots with maxima where the ZB spots should be (see Figure 1c).

We conclude that the C−S NWs exhibit primarily a clean WZ crystal phase besides regions close to the gold catalyst and the bottom, where stacking variations and ZB inclusions occur.

A typical μ-Raman spectrum measured in the center of an individual AlAs−GaAs C−S NWs at room temperature (RT) is depicted in Figure 2a. The polarization of the incoming light was selected parallel to the main NW axis that coincides with the [0001] optic axis. The polarization of the scattered radiation was analyzed parallel to the same axis. Referring to the sketch of Figure 2a, this corresponds to $\bar{x}(z,z)x$ in Porto notation. It is worth noting, that the employed excitation energy of 1.96 eV is close to a predicted direct interband critical point at 1.971 eV that is supposed to arise due to the diversified electronic band structure in WZ AlAs in comparison to its ZB counterpart.[10] At this spatial position, we observe vibrational modes at 266 ± 1, 358 ± 1, and 362 ± 2 cm^{-1}. Here, the error combines the fitting error and the error that originates from the absolute calibration of the spectrometer. For a quantitative analysis, Lorentzian peak fitting of these modes was conducted (fitted curves indicated as red solid lines in Figure 2a).

The mode at 266 ± 1 cm^{-1} coincides with the energy for the A_1(TO) phonon mode of WZ GaAs reported recently.[24,25] Hence, we attribute this particular mode to the WZ GaAs shell surrounding the core and further conclude that no strain is induced within the experimental accuracy due to the GaAs shell.

At higher frequencies, we find a dominating peak at around 358 ± 1 cm^{-1} that we assign to the A_1(TO) mode arising from the WZ AlAs core. The vibrational mode suffers a redshift of 3−5 cm^{-1} with respect to the

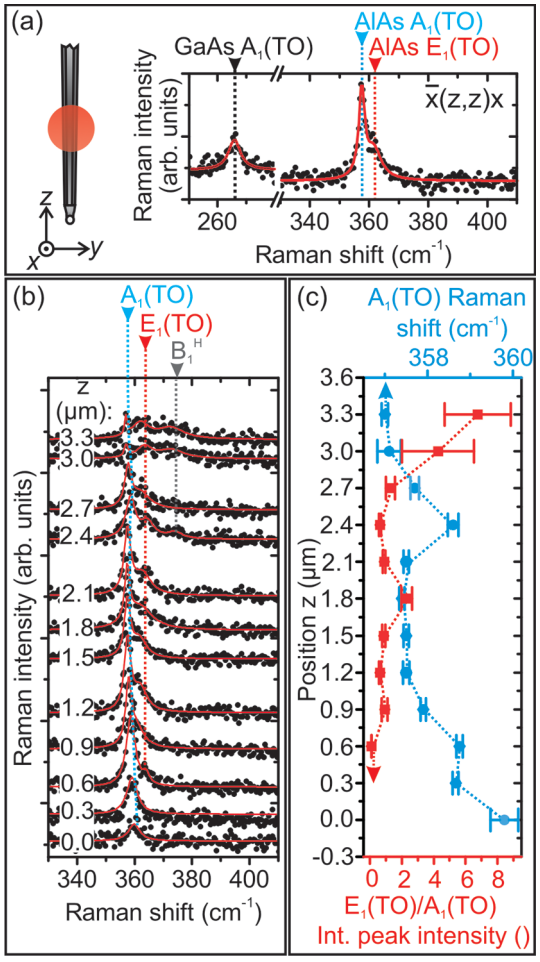

Figure 2. (a) Typical Raman spectrum recorded at the center of an individual AlAs–GaAs C–S NW. (b) Spatially resolved Raman scan along an individual C–S NW where black dots are experimental points and red solid lines are multi-Lorentzian peak fits. Spectra have been shifted vertically for clarity. (c) Peak wavenumbers of the A_1(TO) (blue dots) are correlated with the relative integrated peak intensity of the E_1(TO) (red squares) as a function of the spatial position along an individual C–S NW.

ZB related AlAs TO peak observed in the bulk.[26,27] Group theory and measurements performed on, for example, WZ GaAs NWs show that in the polarized configuration employed only the A_1(TO) mode is allowed in the WZ phase.[25,26,29] In fact, in uniaxial crystals the anisotropy of the crystal results in an anisotropy of the force constants. In Raman scattering this manifests as a spectral A_1–E_1 splitting,[24,28] where the A_1(TO) mode that is polarized along the [0001] crystallographic direction suffers generally a redshift compared to the E_1 (TO) and ZB related TO of the same compound.

Besides the A_1(TO) peak at 358 ± 1 cm^{-1} we find an adjacent spectral feature at 362 ± 2 cm^{-1}. For ZB AlAs in the bulk form, a frequency of 361–363 cm^{-1} was reported for the transversal optical (TO) mode in first-order Raman scattering.[26,27] This value coincides with the mode we observe at 362 ± 2 cm^{-1}. In the case of a WZ crystal, phonon modes of E_1 symmetry arise that

TABLE 1. Wavenumbers of Phonon Modes Expected in WZ AlAs as Well as the Expected Configurations for which Raman Measurements Are Possible Are Compared with the Values and Corresponding Configurations Reported in This Work

	expected[25,29,31]		measured (this work)	
mode	position (cm^{-1})	configuration	position (cm^{-1})	configuration
E_1(LO)	400	$\bar{x}(y,z)y$		
A_1(LO)	<400	$\bar{z}(y,y)z$		
B_1^H	372	silent mode	373 ± 2	$\bar{x}(z,z)x$
E_1(TO)	363	$\bar{x}(y,z)x$, $\bar{x}(z,y)x$, $\bar{x}(y,z)y$, $\bar{x}(z,y)y$	362 ± 2	$\bar{x}(z,z)x$
A_1(TO)	<363	$\bar{x}(z,z)x$, $\bar{x}(y,y)x$	358 ± 1	$\bar{x}(z,z)x$
E_2^H	352	$\bar{x}(y,y)x$, $\bar{x}(y,y)z$, $\bar{z}(y,x)z$, $\bar{z}(y,y)z$		
B_1^L	212	silent mode		
E_2^L	71	$\bar{x}(y,y)x$, $\bar{x}(y,y)z$, $\bar{z}(y,x)z$, $\bar{z}(y,y)z$		

are commonly larger in energy than those of A_1 symmetry and close to the TO mode in ZB due to their polarization perpendicular to the optic axis. In this case, the altered stacking sequence does not affect the force constants to a greater extent. Therefore, we attribute the mode at 362 ± 2 cm^{-1} to a E_1(TO) mode.

To study the influence of stacking variations and ZB inclusions that we detected in our TEM investigations at the extremes of the C–S NWs, we performed spatial scans along individual C–S NWs collecting a spectrum every 300 nm. Notably, the step size is smaller than the spot size of 900 ± 100 nm. Hence, we obtain a convolution of light scattered in overlapping areas. A typical μ-Raman scan is depicted in Figure 2b. At $z > 2.4\ \mu$m, we detect a small contribution of a phonon mode at 373 ± 2 cm^{-1}. Several works have found experimental agreement with vibrational modes of the WZ structure by folding the phonon-wavevector dispersion for the corresponding ZB structure along the [111] direction ($\Gamma \rightarrow$ L).[25,29,30] As a consequence, four new modes appear at the Γ point of the first Brillouin zone. In particular, this results in a phonon mode of B_1^H symmetry that should roughly coincide with the energetic value of the LO mode at the L point of the first Brillouin zone in the ZB phase. For ZB AlAs, a value of 377 cm^{-1} and 372 cm^{-1} was determined for the LO at the L point by second order Raman scattering and *ab initio* calculations, respectively.[27,31] We note that the B_1^H is generally silent in Raman scattering as can be understood from group symmetry considerations but can however be induced by defects such as by the stacking variations that we found in our TEM investigations at the spatial extremes of the NW.[28,30] Hence, we attribute this particular mode at 373 ± 2 cm^{-1} to a disorder activated B_1^H mode in WZ AlAs. To summarize the preceding results, we compare in Table 1 the wavenumbers of phonon modes expected from the

folding of the phonon-wavevector dispersion along the [111] direction[25,29,30] with the values measured in this work. Here, we also indicate the configurations for which Raman measurements are possible together with the configuration employed.[25,28]

Interestingly, we observe an energetic redshift of about 1 cm^{-1} for the A_1(TO) phonon mode at $z >$ 2.4 μm while we find a gradual energetic blueshift of about 2−3 cm^{-1} at the opposite end ($z < 0.9$ μm). We assign both shifts to strain. We think that the different directions of strain at both ends are caused by the axial ZB GaAs segment that is just present at one end. In the case of InAs and InSb nanowires, it has been recently reported that the WZ crystal phase tends to stretch the distances of atomic layers parallel to the *c* axis by 0.4% while those perpendicular are slightly compressed by about 0.2%.[32] A similar trend was observed in the case of WZ AlAs.[19] Hence, the change of crystal phase from WZ to ZB should lead to compressive strain in the WZ part parallel to the *c* axis, that in turn should evoke a blueshift of the A_1(TO) mode since it is polarized along *c*.[28] This agrees with our observations and is supported by the fact that at the same end, we also observe a blueshift of the GaAs TO mode and an increase of its intensity that we indeed attribute to the axial GaAs segment. The slight redshift at the opposite end is less clear. It may be induced by tensile strain caused by breaking the C−S NW off the substrate or crystal defects introduced during the start of the growth.

Resonant Effects and Interband Critical Points. Besides the structural origin of the strain, it is interesting to note the anticorrelation between the peak frequency of the A_1(TO) mode and the relative intensity of the E_1(TO) mode that becomes apparent in Figure 2c. This finding can be understood as follows: Compressive (tensile) strain leads to a blueshift (redshift) of vibrational modes. On similar footing, the electronic band transitions of WZ AlAs blueshift (redshift) due to the energetic change of the underlying electronic Bloch states.

Hence, the excitation energy that has been chosen to be in close resonance with the fundamental bandgap of WZ AlAs that is theoretically expected at 1.97 eV trails off (approaches) this particular resonance and the Raman cross section of distinct vibrational modes reduces (increases). This interpretation is confirmed by temperature-dependent measurements where we cooled the C−S NWs from RT to 15 K. A temperature decrease entails a blueshift of band transitions in crystals and leads to similar physical effects as compressive strain with respect to the energetic position of vibrational and electronic energies. Indeed, we observe an inhibition of the E_1(TO) mode accompanied by a blueshift of the A_1(TO) mode when the temperature is reduced (see Figure 3). This gives evidence of a resonant nature of the E_1(TO) mode for an excitation energy of 1.96 eV at RT and could explain the presence of the E_1(TO) mode that we in fact would not expect for

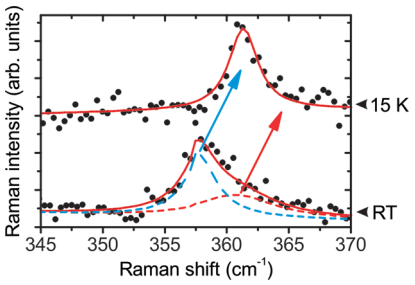

Figure 3. Raman spectra in the center of an individual NW at RT as well as at 15 K. Black dots are experimental points and red solid lines are (multi)-Lorentzian peak fits. In the lower spectrum (RT), blue and red dashed lines mark the individual Lorentzian contributions of the A_1(TO) and E_1(TO) phonon mode, respectively. Blue and red arrows are guides to the eye. Spectra have been shifted vertically for clarity.

the particular polarization we employed: As pointed out in the beginning, both the exciting and analyzed electric field were polarized or analyzed along the optic [0001] axis of the NW. In such a configuration only the A_1(TO) mode should be observed, while the E_1(TO) mode is expected to occur in a configuration where either the analyzed or the incoming electric field is polarized across the NW axis as can be readily calculated by the corresponding Raman tensors (see also Table 1).[28,30] We note that such selection rules are derived under the assumption of scattering events taking place at the Γ point of the first Brillouin zone, where the phonon wavevector transfer *q* equals zero. This $q = 0$ selection rule can be relaxed for instance due to interruptions of the lattice periodicity or due to the small diameter *d* of the nanowire, that implies an uncertainty of the wavevector *q* proportional to $1/d$.[22,33] Such contributions are expected to be small in our case but may become pronounced under conditions where phonon modes are resonantly enhanced.

To further examine the polarization dependence of the AlAs−GaAs C−S NWs we conducted polarization-dependent measurements. We note that no signal could be detected from the NW whenever either the incident or scattered light was polarized or analyzed strictly perpendicular to the NW main axis. We assign this anisotropy to a manifestation of the antenna-like geometry of the nanostructure that displays a diameter much lower than the wavelength of the incident light. In the case of NWs, it has been shown that anisotropic internal field distributions inside of a NW superimpose selection rules that arise due to crystal symmetries.[34,35] In particular, we find an inhibition of phonon modes of E_2 symmetry that we expect to be most intense in Raman spectra with both the incident and the scattered light polarized perpendicular to the NW axis.[28] We depict the measured peak intensities of the A_1(TO) and E_1(TO) in dependence of the angle ϕ of the analyzed polarization of the electric field ε_s with respect to the main NW axis as dots in Figure 4. Here, the polarization of the incoming light ε_i was fixed parallel

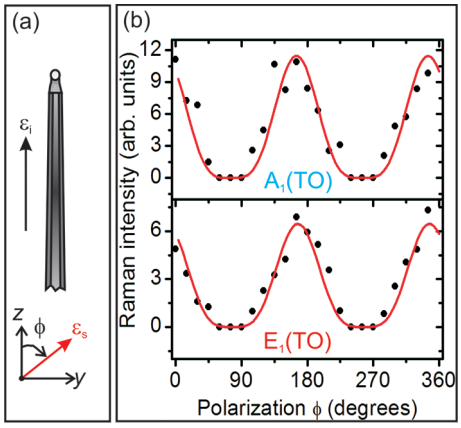

Figure 4. (a) Sketch of the AlAs−GaAs C−S NW with respect to the incoming electric field ε_i and the scattered electric field ε_s analyzed. The angle ϕ depicts the angle of ε_s with respect to the *z*-axis. (b) Measured Raman peak intensities of the A_1(TO) and E_1(TO) phonon modes in dependence of ϕ are shown as black dots. The red solid lines represent $\cos^4\phi$ fits through the data.

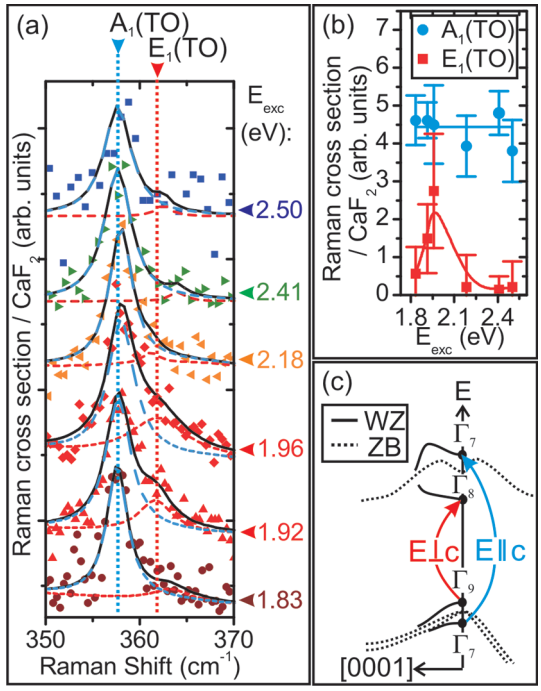

Figure 5. (a) Raman spectra collected in the center of an individual AlAs−GaAs C−S NW in dependence of the excitation energy normalized to CaF_2. Experimental points and multi-Lorentzian fits are depicted as colored symbols and black solid lines, respectively. Lorentzian functions depicted as dashed blue and red lines are individual contributions of the A_1(TO) and E_1(TO) modes, respectively. Spectra have been shifted vertically for clarity. Vertical dashed lines are guides to the eye. (b) Raman cross section of the A_1(TO) and E_1(TO) phonon modes in dependence of the excitation energy. Solid lines are guides to the eye. (c) Sketch of the electronic bandstructure in the proximity of the Γ point of the first Brillouin zone according to ref 10. Allowed optical transitions in dependence of the polarization of the electric field with respect to the optic axis c are indicated.

to the NW axis. As can be seen, the intensity of both modes drops considerably and we cannot resolve them for $\phi > 45$ degrees. The solid lines are $\cos^4(\phi)$ fits that represent the data well with maxima at -13 ± 2 and 167 ± 2 degrees. In an heuristic manner, a $\cos^4(\phi)$ behavior can be decoded combining the Raman tensor of A_1 symmetry—which yields an intensity profile $\propto \cos^2(\phi)$[28,30]—and a depolarization field opposing the incoming and scattered light across the main NW axis. Corresponding results have been obtained modeling internal field distribution for GaP NWs below diameters of 50 nm.[34] In this regard, the A_1(TO) profile *versus* polarization is in agreement with common expectations although we refrain from detailed simulations in the case of AlAs−GaAs C−S NWs at this stage, especially, since theoretical calculations of the dielectric response functions of WZ AlAs[36] have not been confirmed experimentally yet. Surprisingly, the polarization dependence of the E_1(TO) mode follows exactly the one of the A_1(TO) mode within the error of the measurement. A similar argument taking into account the Raman tensor of E_1 symmetry, where classically an intensity profile $\propto \sin^2(\phi)$ is expected,[28,30] should lead to a barely detectable quadrupole-like intensity profile. Again, we conclude that this finding is evidence for a resonant effect. However, it is worth noting that the occurrence of the E_1(TO) mode cannot be explained by internal field distributions due the antenna shape of the C−S NW alone, since we found an inhibition of this mode at cryogenic temperatures, where a considerable change of the dimensions of the NW cannot be expected.

To study the resonance profile of the E_1(TO) phonon mode we performed measurements in dependence of the excitation energy at RT. The polarization of the incoming light was chosen again parallel to the main NW axis. The scattered radiation was also analyzed with a polarization parallel to this axis ($\bar{x}(z,z)x$ and $\phi = 0$, respectively). The spectra have been normalized to the Raman cross section of CaF_2 which is fairly constant in this energy range.[37] We further assume the NW diameter to be much smaller than the attenuation depth of WZ AlAs in the visible spectrum. Hence, we compensate for the influence of dispersive elements in our experimental setup and obtain a signal proportional to the Raman cross section of WZ AlAs.

As can be observed in Figure 5 panels a and b, which show the fitting results for the Raman cross section for the A_1(TO) and E_1(TO) phonon mode, a significant contribution of the E_1(TO) mode is present only in the case of an excitation of 1.92 and 1.96 eV, while for higher or lower excitation energies, this particular mode gets suppressed. This is in agreement with the temperature-dependent measurements, that revealed an extinction of the E_1(TO) for cryogenic temperatures at 1.96 eV. In contrast, the A_1(TO) phonon mode displays no particular resonance between

1.84 and 2.5 eV within the experimental accuracy (see Figure 5b). This can be understood with help of Figure 5c where the expected electronic band structure at the center of the first Brillouin zone of WZ AlAs is sketched: Γ_8 symmetry is predicted for the lowest conduction band at 1.971 eV with respect to the uppermost Γ_9 valence band.[10] An optical transition between those states is allowed perpendicular to the optic [0001] axis only.[38] Since resonant enhancements follow the symmetry of the bands involved in an optical transition,[21] this particular transition cannot couple to a phonon mode of A_1 symmetry that is allowed for polarizations along the optic [0001] axis. In fact, we expect modes of A_1 symmetry to be resonantly enhanced involving bands of the same symmetry. So the corresponding transition would occur between the valence and conduction bands of Γ_7 symmetry with an estimated energetic difference of 3.3 eV which is far above the energies employed in this study. In contrast, E_1 symmetry requires one component of the electric field (either incident or scattered) to be polarized perpendicular to the optic axis. Hence, the cross section of the A_1(TO) mode should appear fairly constant while the E_1(TO) mode depicts a resonance around 2 eV in agreement with our observations. It is worth noting that the $\Gamma_7-\Gamma_8$ transition is forbidden in either polarization and, hence, cannot couple resonantly to any phonon mode.[38]

In resonant cases it is well-known that not only resonant enhancements of the scattering cross section of TO phonon modes can occur but longitudinal optical (LO) modes that are usually forbidden in backscattering from {1100} facets can be activated *via* Fröhlich interaction.[20] Interestingly, we do not observe longitudinal modes of E_1 or A_1 symmetry that we would expect in the proximity of the LO mode at around 400 cm^{-1} in ZB AlAs.[27,31] For the A_1(LO) the same argumentation applies as for the A_1(TO) phonon mode. The suppression of the E_1(LO) on the other hand can be reasoned by another particular property of the Γ_8 conduction band: The band is expected to display a rather large effective mass comparable to the valence band of Γ_9 symmetry.[10] Since the Fröhlich interaction scales with the difference of the inverse effective masses of the bands involved in an optical transition, this effectively reduces the activation of longitudinal modes in WZ AlAs in this energy range.

Interestingly, the observed resonance falls below the X, L, and Γ valleys reported in ZB AlAs at 2.18, 2.35, and 3.03 eV, respectively.[39] This finding suggests a direct nature of WZ AlAs in agreement with recent theoretical calculations. However, the exact energetic positions of valleys apart from the Γ point are experimentally not known for WZ AlAs yet and could compete with the fundamental energy gap below 2.18 eV. More insight into this question would involve a detailed study of photoluminescence (PL) signals which we found to be strongly suppressed in our C−S NW samples. We attribute the suppression to diffusion of photoexcited charge carriers into the GaAs shell and to PL quenching due to the small diameter of the C−S NWs. Additionally, PL backgrounds could be also evoked by the $E_0 + \Delta_0$ split-off band of the GaAs shell that serves as a protection layer of the AlAs core.[39] Such challenges make a detailed PL study difficult at this stage and stress the power of RR spectroscopy when C−S NWs are investigated. In any case, the competition of the Γ valley with adjacent valleys—mainly the M-valley in WZ AlAs[10]—is at least significantly reduced in comparison to the ZB case and could be further tuned by introducing strain or Ga adatoms. We further note that the conduction band structure of, for example, WZ GaP is very similar to AlAs in the WZ phase[11] so that we expect our findings to be applied more generally to semiconductors that in the ZB phase display L valleys at lower energies than the conduction band at the Γ point.

CONCLUSIONS

We presented experimental evidence for an interband critical point below 2.18 eV at the Γ point of the first Brillouin zone of WZ AlAs employing RR spectroscopy. The involved conduction band is found to follow Γ_8 symmetry and to display a high effective mass in agreement with recent theoretical calculations. Furthermore, this finding suggests a direct nature of the fundamental bandgap in this novel material system that could be employed in future nanoscaled optoelectronic systems.

METHODS

AlAs−GaAs C−S NWs were grown by employing the system described in ref 40. To realize large core AlAs NWs suitable for spatial-dependent Raman measurements we have used a two-step growth procedure. In the first step we have grown AlAs NWs at high growth temperature (710 °C) with trimethylaluminium (TMAl) line pressure of 0.4 Torr and tertiarybutylarsine (TBAs) of 4 Torr with a growth time of 4 min. This allows an increase in the catalyst nanoparticle movement on the surface and thereby increases the catalyst agglomeration probability. In a second step we have decreased the growth temperature to 670 °C with TMAl line pressure of 0.2 Torr, TBAs of 4 Torr and with a growth time of 90 min. The reduction of the growth temperature allows an increase in the growth rate, as found in our previous work,[19] while the decrease of the group III flux allows the growth of larger NWs. Owing to the Gibbs−Thomson effect, the smaller catalyst droplets have higher chemical potential, therefore a reduction of group III flux makes it difficult for them to reach the supersaturation condition. Consequently, the growth of small diameter NWs is prevented. To allow for *ex situ* characterization of the AlAs core, the samples were cooled down to a growth temperature of 420 °C under TBAs

flow, and the GaAs shells were grown for 2 min with triethylgallium (TEGa) and TBAs line pressures of 0.7 and 2 Torr, respectively.[19]

Some AlAs NWs were mechanically transferred to carbon-coated copper grids and analyzed by a Zeiss Libra 120 transmission electron microscope (TEM) operating at 120 kV. Core and shell thicknesses were determined on high angle angular dark field scanning TEM images, where the *z* contrast makes the shell clearly visible, and they resulted to be 31 ± 7 nm and 9 ± 1 nm, respectively.

To address individual NWs by μ-Raman spectroscopy, NWs were mechanically transferred to a patterned silicon substrate. Measurements were recorded in a flow-cryostat at 10^{-6} mbar at room temperature as well as at 15 K in backscattering geometry. The 1.96 eV transition of an HeNe laser focused by a microscope objective comprising a numerical aperture = 0.75 was employed as an excitation source. We experimentally determined a spot size of 0.9 ± 0.1 μm in diameter for this particular excitation energy. For the excitation-dependent study we employed several excitation lines arising from Ar^+, Kr^+, and Ar^+/Kr^+ gas and mixed gas lasers at 2.50, 2.41, 2.18, 1.92, and 1.83 eV. The spectra were collected by a XY Dilor triple spectrometer equipped with a multichannel charge coupled device. The spectral resolution of the setup is below 1 cm^{-1} in the entire spectral range we investigate. A low incoming laser power of 40 μW was chosen in order to avoid heating effects. Incoming and scattered light polarizations with respect to the NW main axis were defined by a set of polarization filters and Lambda/2 plates with an error of 10 degrees.

Conflict of Interest: The authors declare no competing financial interest.

Acknowledgment. We kindly thank G. Abstreiter for support and discussion as well as M. Bichler and H. Riedl for excellent technical support. This work was supported financially by the DFG *via* the excellence cluster Nanosystems Initiative Munich (NIM), the Technische Universität München—Institute for Advanced Study, funded by the German Excellence Initiative, and MIUR under PRIN2009 Prot. 2009HS2F7N_003.

REFERENCES AND NOTES

1. Glas, F.; Harmand, J.-C.; Patriarche, G. Why Does Wurtzite Form in Nanowires of III−V Zinc Blende Semiconductors? *Phys. Rev. Lett.* **2007**, *99*, 146101.
2. Akiyama, T.; Sano, K.; Nakamura, K.; Ito, T. An Empirical Approach to Wurtzite−Zinc Blende Polytypism in Group III−V Semiconductor Nanowires. *Jpn. J. Appl. Phys.* **2006**, *9*, L275–L278.
3. Johansson, J.; Bolinsson, J.; Ek, M.; Caroff, P.; Dick, K. A. Combinatorial Approaches to Understanding Polytypism in III−V Nanowires. *ACS Nano* **2012**, *6*, 6142–6149.
4. Spirkoska, D.; Arbiol, J.; Gustafsson, A.; Conesa-Boj, S.; Glas, F.; Zardo, I.; Heigoldt, M.; Gass, M. H.; Bleloch, A. L.; SEstrade, S.; *et al*. A. Structural and Optical Properties of High Quality Zinc-Blende/Wurtzite GaAs Nanowire Heterostructures. *Phys. Rev. B* **2009**, *80*, 245325.
5. Akopian, N.; Patriarche, G.; Liu, L.; Harmand, J.-C.; Zwiller, V. Crystal Phase Quantum Dots. *Nano Lett.* **2010**, *10*, 1198–1201.
6. Dick, K. A.; Thelander, C.; Samuelson, L.; Caroff, P. Crystal Phase Engineering in Single InAs Nanowires. *Nano Lett.* **2010**, *10*, 3494–3499.
7. Ketterer, B.; Heiss, M.; Uccelli, E.; Arbiol, J.; Fontcuberta i Morral, A. Untangling the Electronic Band Structure of Wurtzite GaAs Nanowires by Resonant Raman Spectroscopy. *ACS Nano* **2011**, *5*, 7585–7593.
8. Kusch, P.; Breuer, S.; Ramsteiner, M.; Gelhaar, L.; Riechert, H.; Reich, S. Band Gap of Wurtzite GaAs: A Resonant Raman Study. *Phys. Rev. B* **2012**, *86*, 085317.
9. Koblmueller, G.; Vizbaras, K.; Hertenberger, S.; Bolte, S.; Rudolph, D.; Becker, J.; Döblinger, M.; Amann, M.-C.; Finley, J. J.; Abstreiter, G. Diameter Dependent Optical Emission Properties of InAs Nanowires Grown on Si. *Appl. Phys. Lett.* **2012**, *101*, 053103.
10. De, A.; Pryor, C. E. Predicted Band Structures of III−V Semiconductors in the Wurtzite Phase. *Phys. Rev. B* **2010**, *81*, 155210.
11. Belabbes, A.; Panse, C.; Furthmüller, J.; Bechstedt, F. Electronic Bands of III−V Semiconductor Polytypes and Their Alignment. *Phys. Rev. B* **2012**, *86*, 075208.
12. Bertoni, A.; Royo, M.; Mahawish, F.; Goldoni, G. Electron and Hole Gas in Modulation-Doped GaAs/$Al_{1-x}Ga_xAs$ Radial Heterojunctions. *Phys. Rev. B* **2011**, *84*, 205323.
13. Lucot, D.; Jabeen, F.; Harmand, J.-C.; Patriarche, G.; Giraud, R.; Faini, G.; Mailly, D. Quasi-One-Dimensional Transport in Single GaAs/AlGaAs Core−Shell Nanowires. *Appl. Phys. Lett.* **2011**, *98*, 142114.
14. Spirkoska, D.; Fontcuberta i Morral, A.; Dufouleur, J.; Xie, Q.; Abstreiter, G. Free Standing Modulation Doped Core−Shell GaAs/AlGAAs Hetero-nanowires. *Phys. Status Solidi (RRL)* **2011**, *5*, 353–355.
15. Gallo, E. M.; Chen, G.; Currie, M.; McGuckin, T.; Prete, P.; Lovergine, N.; Nabet, B.; Spanier, J. E. Picosecond Response Times in GaAs/AlGaAs Core/Shell Nanowire-Based Photodetectors. *Appl. Phys. Lett.* **2011**, *98*, 241113.
16. Zhou, H. L.; Hoang, T. B.; Dheeraj, D. L.; Van Helvoort, A. T. J.; Liu, L.; Harmand, J. C.; Fimland, B. O.; Weman, H. Wurtzite GaAs/AlGaAs Core−Shell Nanowires Grown by Molecular Beam Epitaxy. *Nanotechnology* **2009**, *20*, 415701.
17. Chang, C.-C.; Chi, C.-Y.; Yao, M.; Huang, N.; Chen, C.-C.; Theiss, J.; Bushmaker, A. W.; LaLumondiere, S.; Yeh, T.-W.; Povinelli, M. L.; *et al*. Electrical and Optical Characterization of Surface Passivation in GaAs Nanowires. *Nano Lett.* **2012**, *12*, 4484–4489.
18. Yeh, C.-Y.; Wie, S.-H.; Zunger, A. Relationships between the Band Gaps of the Zinc-Blende and Wurtzite Modifications of Semiconductors. *Phys. Rev. B.* **1994**, *50*, 2715–2718.
19. Li, A.; Ercolani, D.; Lugani, L.; Nasi, L.; Rossi, F.; Salviati, G.; Beltram, F.; Sorba, L. Synthesis of AlAs and AlAs−GaAs Core−Shell Nanowires. *Cryst. Growth Des.* **2011**, *11*, 4053–4058.
20. Cardona, M. In *Light Scattering in Solids II: Basic Concepts and Instrumentation*; Cardona, M., Güntherodt, G., Eds.; Springer-Verlag: Berlin, 1982; pp 120−135.
21. Richter, W. In *Springer Tracts in Modern Physics, Vol 78*; Springer: Berlin, Heidelberg, NY, 1976; pp 121−272.
22. Abstreiter, G.; Cardona, M.; Pinczuk, A. Light Scattering by Free Carrier Excitations in Semiconductors. *Top. Appl. Phys.* **1984**, *54*, 5–150.
23. Moeller, M.; De Lima, M. M.; Cantarero, A.; Dacal, L. C. O.; Madureira, J. R.; Iikawa, F.; Chiaramonte, T.; Cotta, M. A. Polarized and Resonant Raman Spectroscopy on Single InAs Nanowires. *Phys. Rev. B* **2011**, *84*, 085318.
24. Crankshaw, S.; Chuang, L. C.; Moewe, M.; Chang-Hasnain, C. Polarized Zone-Center Phonon Modes of Wurtzite GaAs. *Phys. Rev. B* **2010**, *81*, 233303.
25. Zardo, I.; Conesa-Boj, S.; Peiro, F.; Morante, J. R.; Arbiol, J.; Uccelli, E.; Abstreiter, G.; Fontcuberta i Morral, A. Raman Spectroscopy of Wurtzite and Zinc-Blende GaAs Nanowires: Polarization Dependence, Selection Rules, and Strain Effects. *Phys. Rev. B* **2009**, *80*, 245324.
26. Spencer, J.; Grant, R.; Gray, J.; Zolman; Merendez, J. Second-Order Raman Spectroscopy of AlAs: A Test of Lattice-Dynamical Models. *Phys. Rev. B* **1994**, *49*), 5761–5765.
27. J. Wagner, G. S.; Fischer, A.; Braun, W.; Ploog, K. Resonance Effects in First- and Second-Order Raman Scattering from AlAs. *Phys. Rev. B* **1994**, *49*, 7295–7299.
28. Arguello, C. A.; Rousseau, D. L.; Porto, S. P. First-Order Raman Effect in Wurtzite-Type Crystals. *Phys. Rev.* **1969**, *181*, 1352–1363.
29. Harima, H. Properties of GaN and Related Compounds Studied by Means of Raman Scattering. *J. Phys.: Condens. Matter* **2002**, *14*, R967–R993.
30. Hörmann, N. G.; Zardo, I.; Hertenberger, S.; Funk, S.; Bolte, S.; Döblinger, M.; Koblmüller, G.; Abstreiter, G. Effects of Stacking Variations on the Lattice Dynamics of InAs Nanowires. *Phys. Rev. B* **2011**, *84*, 155301.
31. Giannonozzi, P.; De Gironcoli, S.; Pavone, P.; Baroni, S. *Ab Initio* Calculation of Phonon Dispersions in Semiconductors. *Phys. Rev. B* **1991**, *43*, 7231–7242.

32. Kriegner, D.; Panse, C.; Mandl, B.; Dick, K. A.; Keplinger, M.; Persson, J. M.; Caroff, P.; Ercolani, D.; Sorba, L.; Bechstedt, F.; *et al*. Unit Cell Structure of Crystal Polytypes in InAs and InSb Nanowires. *Nano Lett.* **2011**, *11*, 1483–1489.
33. Xiang, Y.; Zardo, I.; Cao, L. Y.; Garma, T.; Heiß, M.; Morante, J. R.; Arbiol, J.; Brongersma, M. L.; Fontcuberta i Morral, A. Spatially Resolved Raman Spectroscopy on Indium-Catalyzed Core−Shell Germanium Nanowires: Size Effects. *Nanotechnology* **2010**, *21*, 105703.
34. Chen, G.; Wu, J.; Lu, W.; Gutierrez, H. R.; Xiong, Q.; Pellen, M. E.; Petko, J. S.; Werner, D. H.; Eklund, P. C. Optical Antenna Effect in Semiconducting Nanowires. *Nano Lett.* **2008**, *8*, 1341–1346(2008).
35. Cao, L.; Laim, L.; Valenzuela, P. D.; Nabet, B.; Spanier, J. E. On the Raman Scattering from Semiconducting Nanowires. *J. Raman Spectrosc.* **2007**, *38*, 697–703.
36. De, A.; Pryor, C. E. Optical Dielectric Functions of Wurtzite III−V Semiconductors. *Phys. Rev. B* **2012**, *85*, 125201(2012).
37. Grimsditch, M.; Cardona, M.; Calleja, J. M.; Meseguer, F. Resonance in the Raman Scattering of CaF_2, SrF_2, BaF_2, and Diamond. *J. Raman Spectrosc.* **1981**, *10*, 77–81.
38. Streitwolf, H. W. Selection Rules for the Space Group C_4^{6v} (Wurtzite). *Phys. Status Solidi* **1969**, *33*, 225.
39. Vurgaftman, I.; Meyer, J. R.; Ram-Mohan, L. R. Band Parameters for III−V Compound Semiconductors and Their Alloys. *J. Appl. Phys.* **2001**, *89*, 5815–5875 and references therein.
40. Ercolani, D.; Rossi, F.; Li, A.; Roddaro, S.; Grillo, V.; Salviati, G.; Beltram, F.; Sorba, L. InAs/InSb Nanowire Heterostructures Grown by Chemical Beam Epitaxy. *Nanotechnology* **2011**, *20*, 505605.